5G millimeter-wave beam adaptation for indoor moving users

5G Millimeter-Wave Beam Adaptation for Indoor Moving Users

R. Schulpen [#1], A. B. Smolders [#], U. Johannsen [#]
[#]Eindhoven University of Technology, the Netherlands
[1]r.schulpen@tue.nl

***Abstract* — This paper presents the results of a preliminary measurement campaign on beam adaptation for indoor moving users, comparing the path loss on a typical modern office floor and a lab floor. The performance of a static user beam is compared to that of an optimized user beam for the scenario of a user walking through a corridor. Results show that beam optimization is most beneficial when a line-of-sight is present. The gain of beam optimization decreases when the number of reflections required to establish a path increases. It is shown that the average path loss after beam optimization is lower on the office floor than on the lab floor that has a similar layout, but mainly metal instead of glass walls. The presented results show that glass walls on the office floor provide low-loss paths via reflections, while a glass window at the lab floor blocks paths.**

***Keywords* — 5G, millimeter-wave propagation, directional antennas, indoor environments, beam steering.**

I. Introduction

Mobile data traffic is forecast to increase by almost eight times by 2023 [1]. This expected growth includes new applications like virtual reality and other video applications, which require very high data rates. The bandwidth scarcity at frequencies below 6 GHz pushes interest to higher frequencies, where more bandwidth is available. The millimeter-wave (mm-wave) band can potentially provide the required bandwidth [2], [3].

Directional communication is essential to compensate for the high propagation losses in the mm-wave band. Due to the small wavelength, large antenna arrays can be used to accommodate beamforming and enable directional communication. The implementation of beamforming in case of moving user equipments (UEs) and dynamical environments is challenging, especially at mm-wave frequencies where humans can block propagation paths. The optimum adaptation rate of the beams depends on many factors like beamwidth, path length, the presence or absence of a line-of-sight (LOS) and the site-specific environment. The beams can be adapted via beam switching, where the base station and UE switch between predefined beams, or via beam steering where the beams are dynamically optimized.

In past years, measurement campaigns on mm-wave indoor propagation and path loss around 28 GHz have been reported (e.g. [4], [5]) as well as measurement campaigns on mm-wave beamforming and beam tracking (e.g. [6], [7]). However, research on beam adaptation for moving users is required to be able to improve antenna array design and beamforming algorithms for 5G mm-wave indoor communication.

Initial results of an indoor measurement campaign on 5G mm-wave beam adaptation for moving UEs are presented and discussed in this paper. The paper is organized as follows. The measurement system used for performing the measurements is described in Section II. Section III provides a detailed description of the measurement scenario. Measurement results are presented and discussed in Section IV. This paper is concluded in Section V.

II. Measurement System

A block diagram of the measurement system is depicted in Fig. 1. A 24.2 GHz continuous-wave (CW) signal is generated by an HP8350B signal generator, amplified by a 20 dB power amplifier (PA) and transmitted using a 17 dBi standard gain horn antenna (SGH). The CW signal is received using an identical SGH, amplified by a 23 dB low noise amplifier (LNA) and detected using a FieldFox N9918A spectrum analyzer. A frequency of 24.2 GHz is used, because it is part of an ISM band that is just below the 24.25-27.5 GHz band, which is the band at the lower end of the mm-wave spectrum that is proposed to be used for 5G in Europe [8].

This measurement system can be used to measure path loss. The effects of frequency drift are mitigated by actively tracking the received signal frequency and updating the center frequency of the spectrum analyzer accordingly. In this way, the sensitivity of the receiver is increased, resulting in a maximum measurable path loss of 150 dB if the antennas are considered part of the measurement system and 116 dB if the antennas are considered part of the channel. 200 snapshots per measurement are averaged to reduce the maximum power variation to less than 1 dB for the whole measurable range down to 10 dB above the noise floor of the receiver, including power variations due to noise, antenna rotation, linearity and temperature variation.

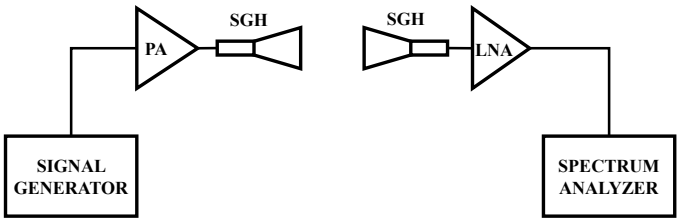

Fig. 1. Block diagram of the measurement system.

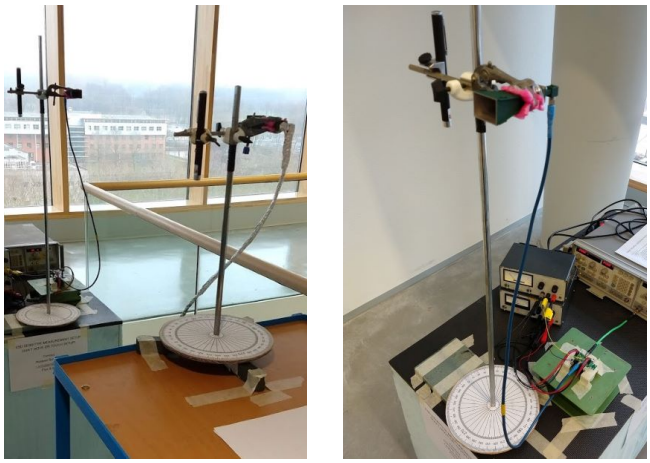

(a) (b)

Fig. 2. Measurement system: (a) OTA calibration setup; (b) Antenna rotation system

A. Calibration

The calibration of the measurement system is similar to the over-the-air (OTA) calibration described in [9]. A reference measurement is taken with a 1 m distance between the apertures of the transmit and receive antennas as depicted in Fig. 2a. For the calibration, a 20 dB attenuator is added to the receiver in order to prevent saturation of the LNA. The measured power in case of the reference measurement can be used to calculate the path loss in dB as

$$\mathrm{PL} = P_{ref} - P_{meas} + FSPL_{1m} + L_{att} - 2 \times G_{SGH} + PC_{cor}, \quad (1)$$

where P_{ref} is the power measured in the 1 m reference measurement, P_{meas} is the measured power during the measurements, $FSPL_{1m}$ is the free-space path loss (FSPL) at 1 m for 24.2 GHz, L_{att} is the precise attenuation of the 20 dB attenuator at 24.2 GHz and G_{SGH} is the antenna gain. PC_{cor} is a correction compensating for the error made in using a 1 m distance between the apertures instead of the phase centers of the antennas [10]. The antennas are considered part of the channel here.

B. Antennas

The 17 dBi SGH antennas have a half-power beamwidth (HPBW) of 24.2° in the H-plane and 24.6° in the V-plane. An approximation of the HPBW of an antenna array consisting of half-wavelength spaced isotropic radiating elements is

$$\mathrm{HPBW} = \frac{1.772}{N} \times \frac{180}{\pi}, \quad (2)$$

where N is the number of antenna elements in the evaluated plane [11]. It can be calculated that the HPBW of the SGHs corresponds roughly to the HPBW of a 4×4 phased array antenna. This is a feasible array size for mm-wave UE antennas and complies with the working assumption for UEs stated in [12].

The antennas are positioned 1.6 m above the floor and a vertical-vertical (V-V) polarization is used during the measurements. The antennas are rotated in azimuth using the manual rotation system depicted in Fig. 2b. A laser pointer is used to determine the antenna rotation with 1° resolution. It is not possible to rotate the antenna around its phase center with this system. Thus fading can vary for different antenna rotation angles.

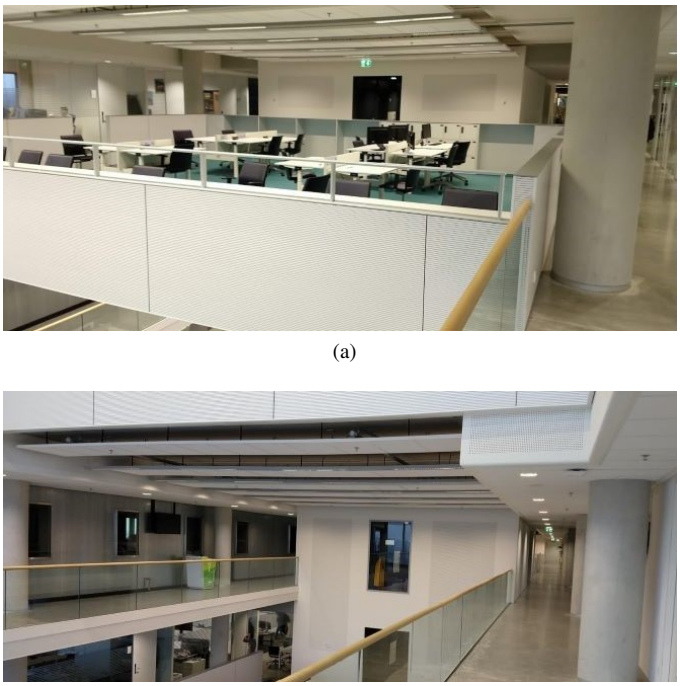

(a)

(b)

Fig. 3. Measurement environments: (a) Office floor; (b) Lab floor

III. Measurement Scenario

The scenario of a mobile user walking down a corridor of an office building, where there is no LOS between the access point (Tx) and UE (Rx) in most instances, is investigated here.

Measurements are conducted at both an office floor (Fig. 3a) and a lab floor (Fig. 3b) in the Flux building of the Eindhoven University of Technology. The corresponding floor plans are depicted in Fig. 4. The office floor is a typical modern office environment with glass wall offices at each side of the building and flexible workspaces in the center. The lab floor has a similar layout as the office floor, but it houses several labs, most with metal walls. There are several concrete pillars in the corridors of both floors. Highly reflecting objects along the track of the moving UE are the middle elevator and four metal fire doors adjacent to the walls at both sides of the corridor. A major difference between the two floors is that at the lab floor, the middle corridor is blocked by a glass window (see Fig. 3b and Fig. 4b).

At both floors, the same measurements are conducted with identical Tx and Rx locations. The measurement scenarios are depicted in Fig. 4. The Rx is moved stepwise through the corridor next to the elevators. Measurements are conducted at ten positions. The distance between the first nine positions is 100 cm, and the distance between position 9 and position 10

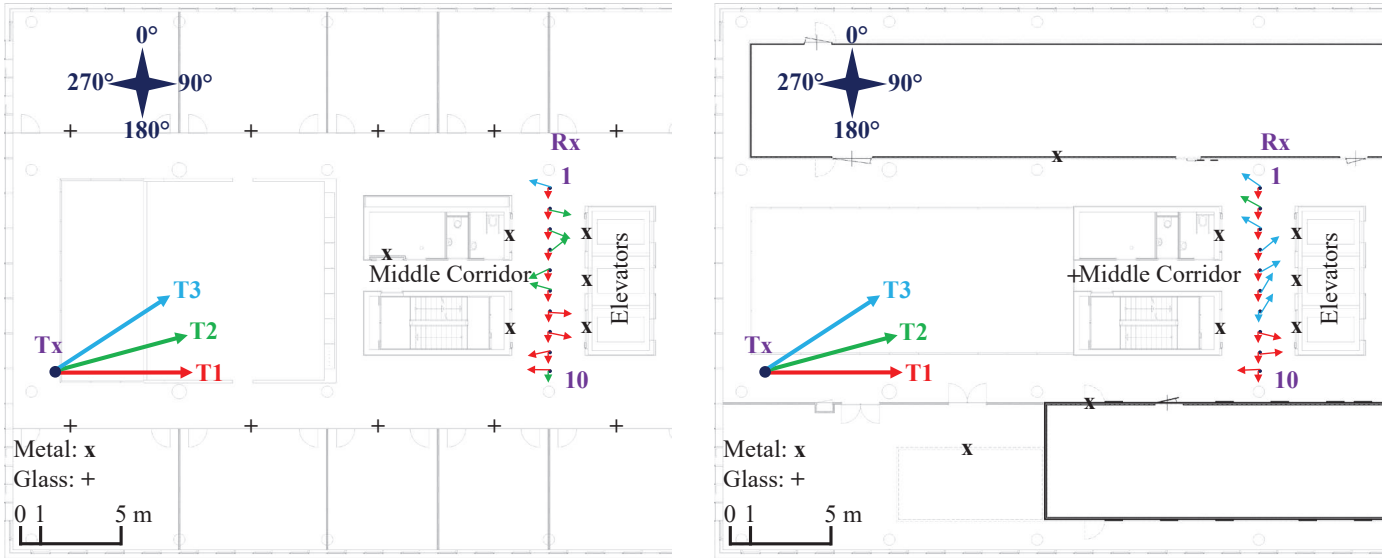

Fig. 4. Floor plans including measurements: (a) Office floor; (b) Lab floor

is 90 cm. A laser distance meter is used to accurately position the Tx and Rx in the same orientation for all measurements and at all measurement positions. Three Tx pointing angles (T1-T3) are evaluated, all pointing to a different corridor. The performance in case of a static Rx beam is compared to that of an optimized Rx beam. The static Rx beam is fixed at 180°, pointing downward in Fig 4a and Fig. 4b. This specific angle is chosen, because in a real-life application of this scenario, the user will be holding his phone in front of him when requiring high data rates enabled by a mm-wave link, for example for video applications. 180° will then be the angle with the least probability of blockage by the user in this scenario. In case of the optimized Rx beam, the Tx-Rx beam combination with the lowest path loss is reported, where the Tx beam is either T1, T2 or T3.

IV. Measurement Results

A visual representation of the measurement results that are discussed below is given in Fig. 4. The directions of the arrows indicate the pointing angles of the antennas for every position for both the static 180° Rx angle and the optimized Rx angle. The colors of the Rx arrows indicate the corresponding Tx beams that provide the paths with the lowest path loss for every position. The results of the static and optimized Rx beams for both the office and lab floor are discussed in Section IV-A and Section IV-B, respectively, and compared in Section IV-C.

A. Static Rx beam

Fig. 5 depicts the path loss for a fixed 180° Rx angle and the three Tx angles for both the office and lab floor. The minimum path loss, using the best Tx angle for every position, is depicted by markers. T1 provides the best path for nine out of ten positions at both floors. This is an expectable result from the 180° Rx angle, which is pointed down the corridor from which the signal from T1 is expected. The average of the minimum path loss over the ten positions is only 3 dB larger in case of the office floor compared to the lab floor. This small difference can be explained by a high reflectivity of the glass walls at the office floor.

Table 1. Optimum beam combinations with corresponding path loss for the optimized Rx beams.

Position	Office			Lab		
	Tx	Rx	PL (dB)	Tx	Rx	PL (dB)
1	T3	287°	61	T3	305°	63
2	T2	103°	62	T2	299°	66
3	T2	112°	63	T3	300°	62
4	T2	52°	58	T3	51°	60
5	T2	245°	64	T3	61°	66
6	T2	286°	55	T3	31°	69
7	T1	94°	61	T3	32°	72
8	T1	102°	61	T1	104°	71
9	T1	258°	58	T1	85°	65
10	T1	271°	50	T1	268°	53

B. Optimized Rx beam

Fig. 6 depicts the path loss for the optimum Rx angle. The minimum path loss in case of the static Rx angle and the theoretical FSPL are depicted for comparison. The theoretical FSPL is the path loss in case of a free-space LOS corresponding to the distance between the Tx and Rx. The Tx and Rx antenna gains of 17 dBi are included in the theoretical FSPL. The optimum Tx-Rx beam combinations and the corresponding path losses are given in Table 1.

A main difference between the office and lab floor is visible in the center of the track, where at the office floor optimum paths are possible via the middle corridor, while at the lab floor these paths are blocked by the glass window there. Another explanation for the lower path loss on the

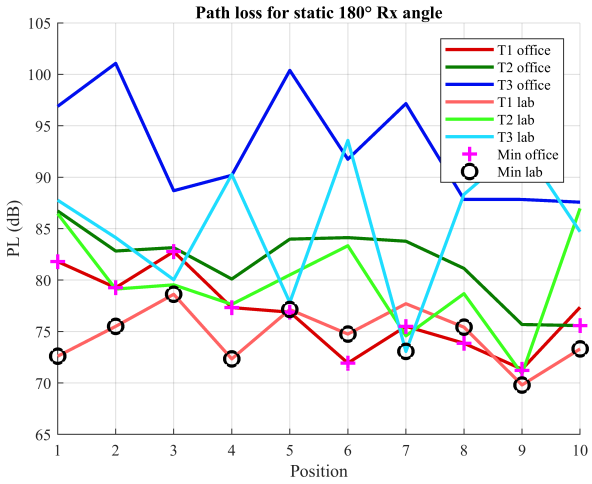

Fig. 5. Path loss for static 180° Rx angle.

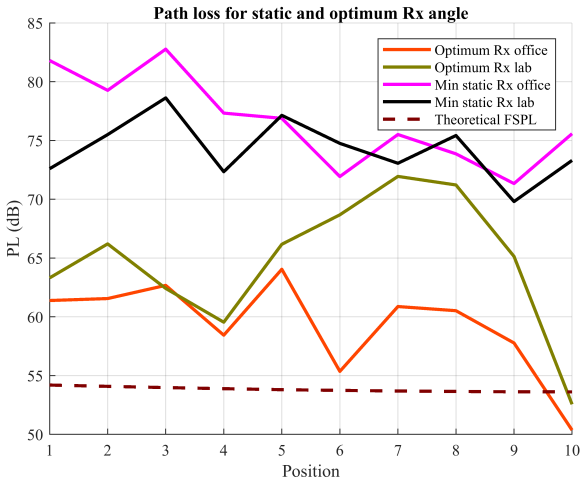

Fig. 6. Path loss for static and optimum Rx angle.

office floor, especially at position 7 and 8, is the presence of wider corridors, which lowers the number of reflections that is required to establish a path between the Tx and Rx. Fig. 4 shows that reflections off the metal fire doors provide optimum paths at several non-line-of-sight (NLOS) positions. At position 10, a LOS link between the Tx and Rx is present, resulting in a path loss less than the theoretical FSPL for both the office and lab floor. This is due to the waveguide effect, where reflected paths off the walls interfere constructively with the direct path at the Rx.

C. Comparison

Fig. 6 shows that an average reduction in path loss of 17 dB can be achieved by optimizing the Rx beam for the office floor, where the difference in path loss between the static and optimized Rx beams is averaged over all ten positions. The average reduction in path loss for the lab floor is 10 dB. The maximum reduction in path loss by optimizing the Rx beam is visible at position 10, where the reduction in path loss compared to the static Rx beam is 25 dB and 21 dB for the office and lab floor, respectively. This can be explained by the LOS link at position 10.

V. Conclusions

The results of a preliminary measurement campaign on mm-wave beam adaptation for indoor moving users are presented in this paper. Although more research is required to be able to draw firm conclusions about the optimum beam adaptation for indoor moving users, this paper already provides insight into factors that can influence the optimum beam adaptation. Beam optimization is most beneficial when a LOS path is present, resulting in a decrease of 25 dB and 21 dB in path loss compared to the static Rx beam for the office and lab floor, respectively. The reduction in path loss by optimizing the Rx beam is smaller when more reflections are required to establish a path between the Tx and Rx. The average path loss after beam optimization is lower on the office floor than on the lab floor, because the glass walls on the office floor provide low-loss paths via reflections, while the glass window in the middle corridor of the lab floor blocks paths.

More research on mm-wave beam adaptation for moving users is needed, including investigations of human blockage and other office environments, and the use of different antenna beamwidths.

Acknowledgment

This work is part of the Flagship Telecom collaboration between KPN and the Eindhoven University of Technology.

References

[1] P. Cerwall *et al.*, "Ericsson mobility report," 2018.
[2] Z. Pi and F. Khan, "An introduction to millimeter-wave mobile broadband systems," *IEEE communications magazine*, vol. 49, no. 6, 2011.
[3] T. S. Rappaport *et al.*, "Millimeter wave mobile communications for 5G cellular: It will work!" *IEEE access*, vol. 1, no. 1, pp. 335–349, 2013.
[4] S. Deng, M. K. Samimi, and T. S. Rappaport, "28 GHz and 73 GHz millimeter-wave indoor propagation measurements and path loss models," in *IEEE International Conference on Communication Workshop (ICCW)*. IEEE, 2015, pp. 1244–1250.
[5] O. H. Koymen, A. Partyka, S. Subramanian, and J. Li, "Indoor mm-wave channel measurements: Comparative study of 2.9 GHz and 29 GHz," in *Global Communications Conference (GLOBECOM)*. IEEE, 2015, pp. 1–6.
[6] W. Roh *et al.*, "Millimeter-wave beamforming as an enabling technology for 5G cellular communications: Theoretical feasibility and prototype results," *IEEE communications magazine*, vol. 52, no. 2, pp. 106–113, 2014.
[7] Y. Inoue *et al.*, "Field experiments on 5G mmw radio access with beam tracking in small cell environments," in *Globecom Workshops*. IEEE, 2015, pp. 1–6.
[8] 3GPP, "TR 38.815 V15.0.0 (2018-06)."
[9] R. Schulpen *et al.*, "Extended range ultra-wideband millimeter-wave channel sounder with over-the-air calibration," in *13th European Conference on Antennas and Propagation (EuCAP)*. IEEE, 2019.
[10] T. Chu and R. Semplak, "Gain of electromagnetic horns," *The Bell System Technical Journal*, vol. 44, no. 3, pp. 527–537, 1965.
[11] R. J. Mailloux, *Phased array antenna handbook*, 2nd ed. Artech house, 2005.
[12] 3GPP, "TR 38.913 V15.0.0 (2018-06)."